

This is the accepted manuscript made available via CHORUS. The article has been published as:

Theory of the Magnetic and Metal-Insulator Transitions in RNiO_3 Bulk and Layered Structures

Bayo Lau and Andrew J. Millis

Phys. Rev. Lett. **110**, 126404 — Published 20 March 2013

DOI: [10.1103/PhysRevLett.110.126404](https://doi.org/10.1103/PhysRevLett.110.126404)

Theory of the magnetic and metal-insulator transitions in $RNiO_3$ bulk and layered structures.

Bayo Lau and Andrew J. Millis

Department of Physics, Columbia University, 538 West 120th Street, New York, NY, USA 10027

A slave rotor-Hartree Fock formalism is presented for studying the properties of the p-d model describing perovskite transition metal oxides, and a flexible and efficient numerical formalism is developed for its solution. The methodology is shown to yield, within an unified formulation, the significant aspects of the rare earth nickelate phase diagram, including the paramagnetic metal state observed for the $LaNiO_3$ and the correct ground-state magnetic order of insulating compounds. It is then used to elucidate ground state changes occurring as morphology is varied from bulk to strained and unstrained thin-film form. For ultrathin films, epitaxial strain and charge-transfer to the apical out-of-plane oxygen sites are shown to have significant impact on the phase diagram.

PACS numbers: 71.30.+h, 73.21.-b, 75.25.-j, 75.25.Dk

Understanding the unusual electronic behavior of transition-metal oxides has been a long-standing question in condensed matter physics,¹ and interest has intensified following the demonstration² that the materials could be used as components of atomically precise oxide heterostructures.^{3–5} The theoretical challenge posed by the materials is to treat, in the many-body context, simultaneously the strong local two-body correlations in the transition metal d -orbitals and their substantial hybridization with oxygen p orbitals. In some systems, the p orbitals can be integrated out and the physics is represented in terms of “ $\hat{U} + \hat{J}$ ” Hubbard model representing the d orbitals only, for which many theoretical methods are available¹. However, in many cases the p -to- d charge transfer is large enough that the p orbitals cannot be neglected. This “negative charge transfer” regime⁶ has been less extensively studied. While much useful information has been provided by density functional theory (DFT)⁷ and its extensions^{8–18}, these methods are computationally intensive, so that the large supercells required for long-period ordered phases are difficult to study. Furthermore, the variety of experimental bulk and superlattice configurations and of many-body phenomena emphasizes the need for a model-system treatment that encapsulates the essential physics so the importance of different contributions can be disentangled.

The rare earth nickelates¹⁹, $RNiO_3$, are an important case in point. Standard valence counting indicates that the electronic ground state (GS) has 7 electrons on each Ni d orbital with fully filled O p orbitals. However, photoemission²⁰ and x-ray absorption^{20–22} experiments, along with unrestricted Hartree-Fock (UHF)^{20,23}, DFT+ U ^{12–14}, and DFT+DMFT¹⁷ calculations, reported that each Ni drains an additional electron from the p orbitals, yielding the $d^8\bar{L}$ configuration, with 8 electrons on the Ni ’s d orbital and 1 electron vacancy on the p orbitals per formula unit, placing the materials in the negative or zero charge transfer gap regime^{6,23}. The physical properties are remarkable: as R is varied across the lanthanum row of the periodic table, the bulk GS changes from paramagnetic metal (PM-M) to correlated

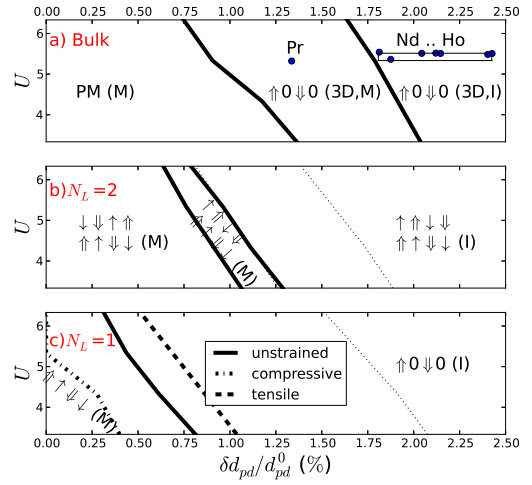


FIG. 1: (a) Bulk, (b) 2-, and (c) 1-layer phase diagram on the u - δd_{pd} plane. In (b,c), the light dotted line indicates the phase boundary obtained without the energy shift on the out-of-layer oxygen. \uparrow/\downarrow denote large moment/small moment/non-magnetic sites of the magnetic patterns. The pattern of (a) is that of Fig. 2b; in (b,c) the symbols denote magnetic pattern of over the x - z plane. Slight charge ordering accompanies the spin ordering for $\delta d_{pd} \neq 0$.

insulator^{1,19,24}. The correlated insulator phases exhibit a rock-salt-pattern lattice distortion^{25–29} and a nontrivial long-period magnetic ordering^{28–33}. In ultra-thin films a metal-insulator transition which is apparently *unaccompanied* by rock-salt-pattern lattice distortion occurs as film thickness and strain are varied^{34–40}. Understanding how these apparently different transitions can occur is an important open theoretical challenge^{9–17,23,40–43}. To the best of our knowledge, none of the previous methods has demonstrated correctly the GS of more than one out of the three scenarios⁴⁴.

In this paper, we develop a mean-field (MF) approach based on a combination of slave-rotor (SR)^{45–49} and Hartree-Fock (HF) methods. The methodology goes beyond previous work by extending the slave-rotor method

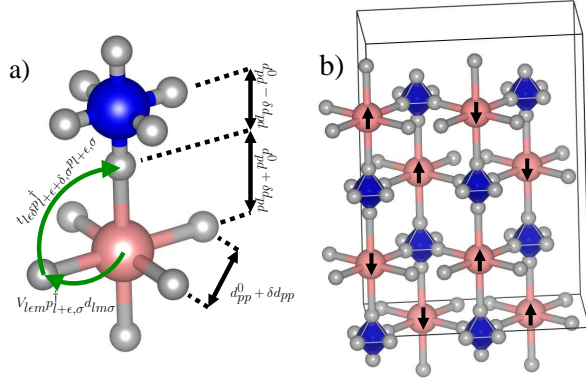


FIG. 2: (a) Hopping (Eq. 2) and geometry of the lattice with rock-salt pattern distortion. Red/blue/gray spheres denote $Ni_{long}/Ni_{short}/O$. (b) The magnetic structure of $\uparrow\uparrow\downarrow\downarrow$ order in the bulk $Ni_{16}O_{48}$ supercell. Ni_{short} forms singlets with its neighboring oxygen sites.

to the charge-transfer (p - d) situation and by performing an unbiased numerical search of large-supercell solutions to the HF+SR equations. It is powerful enough to treat the negative charge transfer physics associated with strong p - d hybridization while permitting the examination of the large supercells needed to investigate long-period ordering patterns. The similarity of our calculated density of states⁴⁴ to that found in DFT+DMFT calculations¹⁷ demonstrates the reliability of the theory. The results reconcile the bulk and film phase diagrams and demonstrate the key role played by the oxygen degrees of freedom and the lattice distortions.

Figure 1 summarizes our key new results as phase diagrams in the space of U (magnitude of correlations on Ni) and δd_{pd} (rocksalt type distortion in Fig. 2a). Fig. 1a shows that, for small or zero δd_{pd} , bulk materials are PM-M at any value of U , consistent with experiment¹⁹. As δd_{pd} increases, transitions occur, first to a magnetic metal and then to a magnetic insulator. The nontrivial ordering wavevector found in experiment²⁸⁻³³ is correctly obtained as a 3D $\uparrow\uparrow\downarrow\downarrow$ pattern (Fig. 2b). States with the $\uparrow\uparrow\downarrow\downarrow$ pattern are unstable against PM or $\uparrow\uparrow\downarrow\downarrow$ solutions, and indeed are not observed in experiments³⁰. In agreement with symmetry arguments⁴³, slight charge ordering always accompanies the spin ordering. For reasonable parameter values the change in electronic structure across the R series is properly accounted for, with one exception: the magnetic metallic phase found in theory is not observed in experiment. This is discussed below. Fig. 1b,c show the evolution of the phase diagram with film thickness N_L and (Fig. 1c) with applied strain, revealing that in ultra-thin films an insulating phase can occur for $\delta d_{pd}=0$. The films' in-plane magnetic patterns resemble a horizontal slice of Fig. 2b, as detailed below.

Our theoretical approach considers the Ni e_g and O $2p_\sigma$ orbitals which were shown to be electronically active by DFT⁹⁻¹⁷. The relevant p - d lattice model is expressed in terms of operators $\hat{H} = \hat{T} + \sum_l (\hat{U}_l + \hat{J}_l)$,

where l sums over the Ni sites. The operator \hat{T} includes the bare energy difference $e_d - e_p$ between the p and d orbitals, in addition to the nearest-neighbor hybridization between p and d orbitals (matrix element V) as well as p and p orbitals (matrix element t). These parameters vary with lattice geometry and the hopping amplitudes $V_{l\sigma m}$ obey the Slater-Koster orbital symmetry factors in Tab. I of Ref. 51. The lattice structure of the $RNiO_3$ materials is derived from the ideal cubic perovskite structure, which is a lattice of corner-sharing oxygen octahedra, each centered at a Ni site. The structure of the actual materials is distorted from ideal structure by rotations of the octahedra which are unimportant for our purposes and, in the insulating cases, by a two-sublattice distortion in which adjacent Ni 's have significantly different Ni -O bond lengths²⁶⁻²⁹. To incorporate the bond disproportionation (Fig. 2a), we scale the hybridization according to the Harrison rule⁵⁰, $V = V^0(1 + \delta d_{pd}/d_{pd}^0)^{-4}$ and $t = t^0(1 + \delta d_{pp}/d_{pp}^0)^{-3}$, with $d_{pd}^0 = 1.95\text{\AA}$ and $d_{pp}^0 = \sqrt{2}d_{pd}^0$. We use l =long/short to denote the location of a Ni site with longer/shorter Ni -O bond length. An additional effect may occur in layered structures. Liu et al.³⁴ showed that the presence of Al at the interface would deplete holes on the out-of-layer oxygen sites linking Al and Ni , raising the charge-transfer energy from those apical sites by $\sim 1\text{eV}$. We model the N_L -layer 2D structures using supercells with N_L NiO_3 units in the z -direction, terminated on both ends with apical oxygen sites whose e_p are shifted by -1eV .

We take the interaction operators \hat{U}_l and \hat{J}_l to have the rotationally invariant Slater-Kanamori form¹. Given in detail in the supplementary material⁴⁴, they are expressed in terms of electron operators $d_{l\sigma}$ and $\hat{n}_l = \sum_{m\sigma} d_{l\sigma}^\dagger d_{l\sigma}$ which operates on spin- σ , $m \in \{d_{z^2}, d_{x^2-y^2}\}$ orbitals at site l . In brief, up to a d -level shift, $\hat{U}_l = \frac{U}{2}\hat{n}_l^2$ is the charging energy controlling the number of particles on Ni site l while \hat{J}_l (scaling with j) differentiates inequivalent configurations among states of the same occupancy. To treat the U term we adopt the slave rotor (SR) approach⁴⁵⁻⁴⁹, devised for the Hubbard model and also applied to other d -only models with Hund's-like interactions^{48,49} under the $j \ll U$ approximation. We extend it here to the p - d model, noting that for $RNiO_3$ $j \sim 1\text{eV}$ is much smaller than either the d - d repulsion and the electron bandwidth. For each e_g site, the approach introduces an auxiliary SR field, $\theta_l \in [0, 2\pi)$, and decomposes electron operators into a pseudofermion f and a phase θ as $d_{l\sigma}^\dagger \rightarrow f_{l\sigma}^\dagger e^{i\theta_l}$. The consistency of SR state and d -occupancy is enforced by the constraint

$$\hat{L}_l = \frac{\partial}{i\partial\theta_l} = \sum_{m\sigma} \left(f_{l\sigma}^\dagger f_{l\sigma} - \frac{1}{2} \right) \quad (1)$$

and we follow previous SR applications and enforce the constraint using Lagrange multipliers, h_l . The \hat{J}_l interactions are written in terms of the f operators as $\tilde{J}_l^{(f)}$ and are treated with the weak coupling Hartree-Fock approxi-

mation, allowing a self-consistent, *unrestricted* treatment of the p - d model under the single-Slater-determinant ansatz $|MF\rangle = |p, f\rangle|\theta\rangle$.

Up to a constant, the system of equations reads

$$\begin{aligned}
 H_{p,f} = & \sum_l J_l^{(f)} + \sum_{lm\sigma} (\Delta - h_l) f_{lm\sigma}^\dagger f_{lm\sigma} \\
 & + \sum_{l\epsilon m\sigma} \langle e^{-i\theta_l} \rangle V_{l\epsilon m} p_{l+\epsilon,\sigma}^\dagger f_{lm\sigma} + h.c. \\
 & + \sum_{l\epsilon\delta\sigma} \frac{t_{l\epsilon\delta}}{2} p_{l+\epsilon+\delta,\sigma}^\dagger p_{l+\epsilon,\sigma}
 \end{aligned} \quad (2)$$

$$H_\theta = \sum_l \frac{U}{2} \hat{L}_l^2 + h_l \hat{L}_l + (e^{i\theta_l} \sum_{\epsilon m\sigma} V_{l\epsilon m} \langle p_{l+\epsilon\sigma}^\dagger f_{lm\sigma} \rangle + h.c.) \quad (3)$$

where Δ is the p - d energy difference plus the d -level-shift arising from the partitioning of the U interaction and $\epsilon\delta$ sum over nearest p - d and p - p neighbors (Fig. 2a). Note that $\langle e^{i\theta_l} \rangle$ is a self-consistently determined number between 1 and 0. A small value signals strong ‘‘Brinkman-Rice’’⁵² renormalization of the bandwidth^{45–47}.

A 3D Bravais lattice of $Ni_{16}O_{48}$ supercells (Fig. 2b) is required for unrestricted modeling of the $(1/2, 0, 1/2)$ pattern with respect to the orthorhombic unit cell. To systematically capture dimensionality effects, we model the N_L -layer structures using a 2D Bravais lattice of $Ni_{4N_L}O_{12N_L+4}$ supercells, which is connected to the 3D $Ni_{16}O_{48}$ supercell for $N_L \rightarrow \infty$. The system is solved by a T=0 iterative procedure for up to 65536 supercells. Without much optimization, the worst case initial condition with bi-partite charge-, orbital-, and magnetic-order would converge into a PM-M or $(1/2, 0, 1/2)$ -ordered insulator within 30 cpu hours on an Opteron-2350 cluster.

The parameters may be obtained from, e.g. maximally localized Wannier fits to DFT results⁵³, but the precise form is not important here (see Ref. 54 for example of the insensitivity of results to the precise p - d model band parameters). We perform bulk calculations for (U, Δ) such that per- Ni d -occupation $n_l = \langle \hat{n}_{lm\sigma} \rangle \sim 2$ as found in UHF with parameters fitted to photoemission spectrum²³, DFT^{12–14}, and DMFT+DFT¹⁷. For the reference set of $U = 5.3$, $j = 1$, $V_{l\epsilon, d_{x^2-y^2}}^0 = 1.5$, $t^0 = 0.5$, $e_d - e_p = -5$, the undistorted 3D lattice has $n_l \sim 1.95$, slightly less than those of the above calculations. To isolate dimensionality effects, we use the bulk’s (U, e_d) pairs, in addition to the aforementioned apical e_p shift, for layered calculations.

The left panel of Fig. 3 shows representative results for the energies of different locally stable phases computed at interaction $(U, j) = (5.3, 1)$ as a function of $(\delta d_{pd})^2$. We see that in agreement with experiment, the lattice with no disproportionation is a PM-M. As disproportionation δd_{pd} is increased a transition to a period-4 metallic magnetic state occurs. At yet larger distortion a metal-insulator transition occurs. The incorrect ferromagnetic (FM) GS found in UHF^{20,23}, DFT+U^{12–14} and

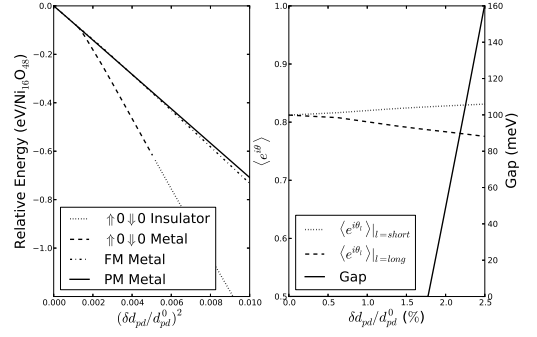


FIG. 3: (Left) Energy of stable solutions of mean field theory measured relative to ground state of undistorted bulk system. (Right) rotor renormalization and insulating gap for the bulk system at $U = 5.3$.

DFT+DMFT¹⁷ become locally stable only at larger δd_{pd} and gain less energy than does the experimentally observed ordering pattern. Also, $E \sim -\delta d_{pd}^2$ implies an equilibrium distortion determined by the anharmonic lattice restoration force beyond the scope of this study.

We now examine the role of \hat{U} correlation in the formalism. The right panel of Fig. 3 shows the $\langle e^{i\theta_l} \rangle$ values on the l =long/short sublattices. We see that the renormalizations are not large, and are only weakly dependent on sublattice, thus showing that the $d^8\bar{L}$ configuration is far from the conventional Brinkman-Rice transition⁵². This renormalization has a moderate effect on physical properties, e.g. Fermi velocity is reduced by 35% in the PM-M at $(U, j) = (5.3, 1)$. Even then, the renormalized kinetic terms, combined with lattice distortion and the magnetic order opens a gap in the density of states. We stress that the $U \neq 0$ renormalization $\langle e^{i\theta_l} \rangle$ is required for insulation.

Parameters scaled for different R bulk materials^{26–29} are marked on Fig. 1a. We see that the theory captures all experimentally observed phases over the R series, with the exception of $R = Pr$, which is predicted to be a metal instead of an insulator, albeit with the correct charge and magnetic order. This can be understood by noting that our approach underestimates the insulating gap⁴⁴, which is 160meV at $\frac{\delta d_{pd}}{d_{pd}^0} = 2.5\%$ compared to ~ 200 meV in a 2-site DFT+DMFT study¹⁷, and that $R = Pr$ is also extrapolated to be a metal from those $R = Lu$ results.

In agreement with experiments, the $\uparrow 0 \downarrow 0$ insulator (Fig. 2b) has a $(1/2, 0, 1/2)$ magnetic structure with respect to the orthorhombic unit cell, a rock-salt charge ordering pattern, but without orbital ordering. Consider the $\frac{\delta d_{pd}}{d_{pd}^0} = 2.5\%$ solution. The sites d -occupancies are $n_{\text{long}} (n_{\text{short}}) = 2.03 (1.90)$. This disproportionation can be understood by measuring the Ni - O hybridization order parameter $\hat{\tau}_l = \sum_{\epsilon m\sigma} V_{l\epsilon m}^0 e^{-i\theta_l} p_{l+\epsilon\sigma}^\dagger f_{lm\sigma} + h.c.$ We found that $\frac{\langle \tau_{\text{short}} \rangle}{\langle \tau_{\text{long}} \rangle} = 1.4$, which is greater than expected from the $\sim 10\%$ hopping modulation. This shows

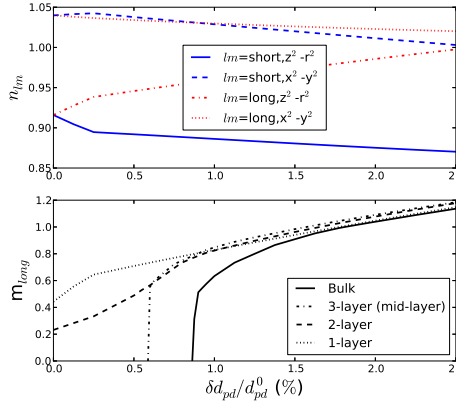


FIG. 4: Results for $U = 5.3$. (Top) $n_{lm} = \sum_{\sigma} \langle n_{lm\sigma} \rangle$ for the 1-layer structure. (Bottom) m_{long} magnetic moment for bulk, middle layer of 3-layer, 2- and 1-layer structures.

that Ni_{short} is strongly hybridized with p orbitals while Ni_{long} retains its d^8 characteristic. The magnetic moments are $m_{long}=1.1$, which agrees with experiment^{28,29}, and $m_{short}=0$. This unusual ordering pattern arises from the unusual properties of the negative charge transfer limit: in the $d^8 \underline{L}$ configuration, the effective physics of strong p - d hybridization is a strong antiferromagnetic p - d spin correlation which leads to singlet formation on the short-bond sites with antiferromagnetically correlated $S = 1$ on the long-bond sites. The formation of p - d singlets has also been reported in DFT+DMFT¹⁷.

We now discuss the effects of dimensional confinement. The bulk and $N_L \geq 3$ layers structures have similar phase diagrams, with enlarging ordered and insulating region for decreasing N_L and increasing U . In particular, the lower panel of Fig. 4 shows that PM-M exists for $N_L \geq 3$. The phase diagram of 2- and 1-layer films are shown in Fig. 1b,c. We see that, for $M \leq 2$ layers, the ground state is always magnetically ordered, even without distortions. Further, the distortion required for the transition to the insulating phase decreases with increasing U and decreasing N_L . At $(U, j)=(5.3, 1)$, the metal-insulator boundary $(\frac{\delta d_{pd}}{d_{pd}^0})_{MIT}$ is reduced from 1.9% to 0.96% and 0.44% for 2- and 1-layer, respectively. A comparison between the solid and dotted lines in Fig. 1c shows that charge transfer to the out-of-plane orbitals³⁴ greatly enlarge the insulating regions.

To study the effects of epitaxial strain, we focus on 1-layer structure for concreteness. We include the strain effects by scaling hopping integrals according to the Harrison rule⁵⁰ for the geometry specified in Ref. 39, which introduced compressive (tensile) strain with $LaSrAlO_4$ ($SrTiO_3$) such that the lattice parameters are $a=b=3.769$ (3.853) Å and $c = 3.853$ (3.790) Å. Breathing-mode distortion is then introduced as before. In agreement with ultra-thin-film experiments^{35,36,39}, Fig. 1c shows that compressive (tensile) epitaxial strain enlarges (shrinks) the insulating region. Under realistic values of U and compressive stain, ordered insulator is possible for

$\delta d_{pd}=0$, agreeing with experiments which so far found breathing-mode distortion only under tensile strain⁴⁰. Note that further shift in apical oxygen e_p also decreases δd_{pd} required for insulation.

Figure 4 demonstrates an orbital polarization of $\sim 5\%$. We also found that the polarization decreases (increases) with compressive (tensile) strain, in agreement with a DFT+U study^{11,12}. For example, $LaSrAlO_4$ ($SrTiO_3$) substrate changes the polarization to ~ 4 (6)%. While DFT+U predicted FM order, our $N_L=1,2$ GS have an AFM in-plane order of $\uparrow\uparrow\downarrow\downarrow$, which differs slightly from a horizontal slice of Fig. 2b by having small $m_{short} \neq 0$ which decreases with increasing distortion. The 2-layer structure has an additional magnetic transition between FM and AFM ordering in the z -direction (Fig. 1b).

To gain additional insight into the physics of our results we compare them to previous studies of other models. Cluster DMFT methods provide in principle a better treatment of the many-body physics, but are so computationally intensive that the large-period superlattices studied here have not been treated by these methods. As previously noted, for the paramagnetic case the local density of states obtained by our methods is in good agreement with those obtained by DMFT. Our bulk PM-M develops into $\uparrow 0 \downarrow 0$ -I for $\frac{\delta d_{pd}}{d_{pd}^0} > 1.9\%$ compared to UHF's $\frac{\delta d_{pd}}{d_{pd}^0} > 7.5\%$ transition from FM to MCO state with similar pattern²³. This difference arises from the charge fluctuation effects treated by the rotor approximation. Calculations in the d -only model in the region reveal an S-SDW state with the same wave-vector as found here, but a different distribution of spin magnitudes; but in the d -only model this state is found only in the unphysically large $j/U > 1$ region⁴¹. Also unlike the results reported for the d -only model⁴¹, our results are sensitive to dimensional confinement. Different DFT implementations have been employed to capture the bulk $LaNiO_3$ PM-M¹⁵ and $LaNiO_3/LaAlO_3$ ordered insulating layer¹⁶, but the demonstration of all bulk and layered phases by a single formulation had been elusive to the best of our knowledge.

Our formulation bridges the gap between HF-like approaches and the expensive cluster DMFT. The results connect all $RNiO_3$ phases in bulk and layer form and provide detailed insights in particular into the importance of charge transfer to oxygen, which is seen to be essential to the results. We suggest that the method provides a viable pathway for treating systems with different superstructures as well as compounds such as Fe and Co oxides with strong p - d hybridization and large number of partially filled strongly correlated orbitals. For example, Sr_2FeO_4 has also been shown to exhibit strong hybridization and non-trivial magnetic order⁵⁵.

We thank G. A. Sawatzky, H. Chen, H. T. Dang, R. Fernandez, S. Park, and D. Zgid for helpful discussions. This work is supported by US Department of Energy DOE grant ER-046169.

- ¹ M. Imada, A. Fujimori, and Y. Tokura, *Rev. Mod. Phys.* **70**, 1039 (1998)
- ² Ohtomo, A., Muller, D. A., Grazul, J. L. and Hwang, H. Y., *Nature* **419**, 378380 (2002).
- ³ Mannhart, J., Blank, D. H. A., Hwang, H. Y., Millis, A. J. and Triscone, J. -M., *M. R. S. Bulletin*, **33** 1027-34, (2008).
- ⁴ H. Y. Hwang, Y. Iwasa, M. Kawasaki, B. Keimer, N. Nagaosa and Y. Tokura, *Nature Materials* **11** 103 (2012)
- ⁵ J. Chakhalian, A. J. Millis and J. Rondinelli, *Nature Materials*, **11** 92-94 (2012)
- ⁶ J. Zaanen, G. A. Sawatzky, and J. W. Allen, *Phys. Rev. Lett.* **55** 418 (1985)
- ⁷ R. O. Jones and O. Gunnarsson, *Rev. Mod. Phys.* **61**, 689–746, (1989).
- ⁸ V. I. Anisimov, I. V. Solovyev, M. A. Korotin, M. T. Czyzyk, and G. A. Sawatzky *Phys. Rev. B* **48** 16929 (1993)
- ⁹ G. Giovannetti, S. Kumar, D. Khomskii, S. Picozzi, and J. van denBrink, *Phys. Rev. Lett.* **103** 156401 (2009)
- ¹⁰ S. Prosandeev, L. Bellaiche, and Jorge Iñiguez, *Phys. Rev. B* **85** 214431 (2012); in particular, footnote 15.
- ¹¹ M. J. Han and M. van Veendaal *Phys. Rev. B* **84** 125137 (2011)
- ¹² M. J. Han and M. van Veendaal *Phys. Rev. B* **85** 195102 (2012)
- ¹³ Ariadna Blanca-Romero and Rossitza Pentcheva *Phys. Rev. B* **84** 195450 (2011)
- ¹⁴ V Anisimov, D Bukhvalov, and T Rice, *Phys. Rev. B* **59** 7901 (1999)
- ¹⁵ G. Gou, I. Grinberg, Andrew M. Rappe, and J. M. Rondinelli *Phys. Rev. B* **84**, 144101 (2011)
- ¹⁶ D Puggioni, A Filippetti, and V Fiorentini, *arxiv:1203.2066* (2012)
- ¹⁷ H. Park, A. J. Millis, C. A. Marianetti, *arxiv:1206.2822* (2012)
- ¹⁸ G. Kotliar, S. Y. Savrasov, K. Haule, V. S. Oudovenko, O. Parcollet, and C. A. Marianetti, *Rev. Mod. Phys.* **78** 865 (2006)
- ¹⁹ M L Medarde *J. Phys.: Condens. Matter* **9** 1679 (1997)
- ²⁰ T. Mizokawa, A. Fujimori, T. Arima, Y. Tokura, N. Mori, and J. Akimitsu, *Phys. Rev. B* **52** 13865(1995)
- ²¹ M. Abbate, G. Zampieri, F. Prado, A. Caneiro, J. M. Gonzalez-Calbet, and M. Vallet-Regi, *Phys. Rev. B* **65** 155101 (2002)
- ²² K. Horiba, R. Eguchi, M. Taguchi, A. Chainani, A. Kikkawa, Y. Senba, H. Ohashi, and S. Shin, *Phys. Rev. B* **76** 155104 (2007)
- ²³ T. Mizokawa, D. I. Khomskii, and G. A. Sawatzky, *Phys. Rev. B* **61** 11263 (2000)
- ²⁴ J. B. Torrance, P. Lacorre, A. I. Nazzal, E. J. Ansaldo, Ch. Niedermayer, *Phys. Rev. B* **45** 8209 (1992)
- ²⁵ M. Medarde, C. Dallera, M. Grioni, B. Delley, F. Vernay, J. Mesot, M. Sikora, J. A. Alonso, and M. J. Martinez-Lope, *Phys. Rev. B* **80** 245105 (2009)
- ²⁶ M. Medarde, M. T. Fernandez-Diaz, and P. Lacorre, *Phys. Rev. B* **78**, 212101 (2008)
- ²⁷ J. L. Garcia-Munoz, M. A. G. Aranda, J. A. Alonso and M. J. Martinez-Lope, *Phys. Rev. B* **79** 134432 (2009)
- ²⁸ J. A. Alonso, J. L. Garcia-Munoz, M. T. Fernandez-Diaz, M. A. G. Aranda, M. J. Martinez-Lope, and M. T. Casais, *Phys. Rev. Lett.* **82** 3871 (1999)
- ²⁹ J. A. Alonso, M. J. Martinez-Lope, M. T. Casais, J. L. Garcia-Munoz, M. T. Fernandez-Diaz *Phys. Rev. B* **61** 1756 (2000)
- ³⁰ V. Scagnoli, U. Staub, A. M. Mulders, M. Janousch, G. I. Meijer, G. Hammerl, J. M. Tonnerre, and N. Stojic, *Phys. Rev. B* **73** 100409(R) (2006)
- ³¹ V. Scagnoli, U. Staub, Y. Bodenthin, M. Garcia-Fernandez, A. M. Mulders, G. I. Meijer and G. Hammerl, *Phys. Rev. B* **77** 115138 (2008)
- ³² J. L. Garcia-Munoz, J. Rodriguez-Carvajal, and P. Lacorre, *Phys. Rev. B* **50** 978 (1994)
- ³³ Y Bodenthin, U Staub, C Piamonteze, M Garcia-Fernandez, M J Martinez-Lope, J A Alonso, *Journal of Physics Condensed Matter* **23**, 036002 (2011)
- ³⁴ J. Liu, S. Okamoto, M. van Veenendaal, M. Kareev, B. Gray, P. Ryan, J. W. Freeland, and J. Chakhalian, *Phys. Rev. B* **83** 161102 (2011)
- ³⁵ J. Liu, M. Kareev, D. Meyers, B. Gray, P. Ryan, J. W. Freeland, and J. Chakhalian, *Phys. Rev. Lett.* **109** 107402 (2012)
- ³⁶ E.J. Moon, B.A. Gray, M. Kareev, J. Liu, S.G. Altendorf, F. Strigari, L.H. Tjeng, J.W. Freeland, J. Chakhalian, *arxiv:1105.5602* (2012)
- ³⁷ J. Son, P. Moetakef, J. M. LeBeau, D. Ouellette, L. Balents, S. James Allen, and S. Stemmer *Appl. Phys. Lett.* **96**, 062114 (2010)
- ³⁸ J. Son, J. M. LeBeau, S. J. Allen, and S. Stemmer, *Appl. Phys. Lett.* **97**, 202109 (2010)
- ³⁹ A. V. Boris, Y. Matiks, E. Benckiser, A. Frano, P. Popovich, V. Hinkov, P. Wochner, M. Castro-Colin, E. De-temple, V. K. Malik, C. Bernhard, T. Prokscha, A. Suter, Z. Salman, E. Morenzoni, G. Cristiani, H.-U. Habermeyer, and B. Keimer, *Science* **332** 937 (2011) and the Supplementary material therein.
- ⁴⁰ J. Chakhalian, J. M. Rondinelli, Jian Liu, B. A. Gray, M. Kareev, E. J. Moon, N. Prasai, J. L. Cohn, M. Varela, I. C. Tung, M. J. Bedzyk, S. G. Altendorf, F. Strigari, B. Dabrowski, L. H. Tjeng, P. J. Ryan, and J. W. Freeland, *Phys. Rev. Lett.* **107** 116805 (2011).
- ⁴¹ S. Lee, R. Chen, and L. Balents, *Phys. Rev. B* **84** 165119 (2011)
- ⁴² I. I. Mazin, D. I. Khomskii, R. Lengsdorf, J. A. Alonso, W. G. Marshall, R. M. Ibberson, A. Podlesnyak, M. J. Martinez-Lope, and M. M. Abd-Elmeguid, *Phys. Rev. Lett.* **98** 176406 (2007)
- ⁴³ S. Lee, R. Chen, and L. Balents, *Phys. Rev. Lett.* **106** 016405 (2011)
- ⁴⁴ See Supplementary Materials.
- ⁴⁵ S. Florens and A. Georges *Phys. Rev. B* **70** 035114 (2004)
- ⁴⁶ J. G. Rau and H-Y Kee, *Phys. Rev. Lett.* **106** 056405 (2011)
- ⁴⁷ R. Yu, J-X Zhu, and Q. Si, *Phys. Rev. Lett.* **106** 186401 (2011)
- ⁴⁸ E. Zhao and A. Paramekanti, *Phys. Rev. B* **76** 195101(2007)
- ⁴⁹ W-H Ko and P. A. Lee *Phys. Rev. B* **83** 134515 (2011)
- ⁵⁰ W A Harrison, *Elementary Electronic Structure* (1999)
- ⁵¹ J. C. Slater and G. F. Koster *Phys. Rev.* **94** 1498 (1954)
- ⁵² W. F. Brinkman and T. M. Rice *Phys. Rev. B* **2** 4302 (1970)
- ⁵³ N Marzari and D Vanderbilt *Phys. Rev. B* **56** 12847 (1997)
- ⁵⁴ X. Wang, M. J. Han, L. de Medici, C. A. Marianetti, and A. J. Millis *arxiv:1110.2782* (2011)

- ⁵⁵ G. Kh. Rozenberg, A. P. Milner, M. P. Pasternak, G. R. Hearne, and R. D. Taylor, Phys. Rev. B 58 10283 (1998)